Exploring pseudo-Nambu–Goldstone bosons by stimulated photon colliders in the mass range 0.1 eV to 10 keV

Kensuke Homma[1,2] and Yuichi Toyota[1]

[1]*Graduate School of Science, Hiroshima University, Kagamiyama, Higashi-Hiroshima, Hiroshima 739-8526, Japan*
[2]*International Center for Zetta-Exawatt Science and Technology, Ecole Polytechnique, Route de Saclay, F-91128 Palaiseau Cedex, France*

(Dated: January 17, 2017)

Searching for pseudo-Nambu–Goldstone bosons (pNGBs) in weak-coupling domains is crucial for understanding the dark components in the universe. We propose searching for pNGBs coupled to two photons in the mass range from 0.1 eV to 10 keV. This could provide opportunities to test string-theory-based pNGBs beyond the GUT scale $M \sim 10^{16}$ GeV included in the weak coupling proportional to M^{-1}. We provide formulae that are applicable to photon–photon scattering via a pNGB resonance exchange with a stimulation process in an asymmetric head-on photon–photon collider by mixing three laser pulses in laboratory experiments. We discuss the quantum electrodynamic effects on the pNGB exchange in the same mass–coupling domain as a background process from the standard model. We find that a large unexplored mass–coupling domain is accessible by combining existing laser facilities, including free-electron lasers.

arXiv:1701.04282v1 [hep-ph] 16 Jan 2017

I. INTRODUCTION

Spontaneous symmetry breaking could be one of the most robust guiding principles for general discussions of dark components in the universe. Whenever a global symmetry is broken, a massless boson may appear as a Nambu–Goldstone boson (NGB). In nature, however, an NGB emerges as a pseudo-NGB (pNGB) with a finite mass. Even if a pNGB is close to being massless, its decay into lighter particles such as photons is kinematically allowed. The neutral pion is such an example of a pNGB via chiral symmetry breaking. The effective interaction Lagrangian is defined as

$$-\mathcal{L} = gM^{-1}\frac{1}{4}F_{\mu\nu}F^{\mu\nu}\phi, \tag{1}$$

where we assume a scalar-type field ϕ for simplicity, and M has the dimension of energy whereas g is a dimensionless constant.

There are several theoretical models that predict low-mass pNGBs such as axions [1], dilatons [2], and string-theory-based axion-like particles [3]. However, pinning down the physical mass of a pNGB by means of such models is commonly non-trivial. Therefore, experiments are indispensable for investigating the physical mass as widely as possible in the lower mass range.

We have previously advocated a novel method [4] for stimulating $\gamma\gamma \to \phi \to \gamma\gamma$ scattering in a quasi-parallel collision system (QPS) via an s-channel resonant pNGB exchange by utilizing the coherent nature of laser fields. Kinematically, this is analogous to four-wave mixing in matter [5] if the nonlinear atomic process is replaced with the pNGB exchange. A QPS is intended for searching for pNGBs in the sub-eV mass range. Indeed, we have performed two previous laboratory searches [6, 7] based on this approach.

Recently, an unidentified emission line, $\omega \sim 3.5$ keV, has been reported in the photon energy spectra from a single galaxy and galaxy clusters [8, 9], and the arguments are still actively ongoing [10]. The possible interpretation of a pNGB decaying into two photons has been discussed [11]. Indeed, string theories predict pNGBs to be homogeneously distributed on a log scale in the mass range possibly up to 10^8 eV [3]. This situation motivates us to try to extend the same method up to 10 keV in general. Given the effective Lagrangian $\mathcal{L}$, we evaluate the sensitivity to $\gamma\gamma \to \phi \to \gamma\gamma$ scattering by means of stimulation using coherent X-ray sources. However, we emphasize that the formulae we provide here are nevertheless applicable to a wide mass range from 0.1 eV to 10 keV by combining different types of coherent and incoherent light sources. This mass range is yet to be probed intensively, and thus the proposed approach will open a window through which to explore string-theory-based pNGBs beyond the GUT scale $M \sim 10^{16}$ GeV.

II. FORMULAE FOR STIMULATED ASYMMETRIC PHOTON–PHOTON SCATTERING VIA PNGBS

To distinguish clearly between the photons in the colliding beams and the signal photons whose frequencies have been shifted by the scattering process, we consider an asymmetric collision system (ACS) as illustrated in Fig. 1. The ACS is obtained by boosting a center-of-mass system (CMS) along the head-on collision axis (z axis) with a speed βc, where c is the speed of light (hence, the Lorentz factor is $\gamma = 1/\sqrt{1-\beta^2}$). Four-momenta in the ACS are defined as

$$\begin{aligned} &p_1 = \omega_1(1,0,0,1), p_2 = \omega_2(1,0,0,-1), \\ &p_3 = \omega_3(1,\sin\theta_3,0,\cos\theta_3), p_4 = \omega_4(1,\sin\theta_4,0,-\cos\theta_4). \end{aligned} \tag{2}$$

For later convenience, with an incident photon energy ω in the CMS, we define the incident energies in the ACS as

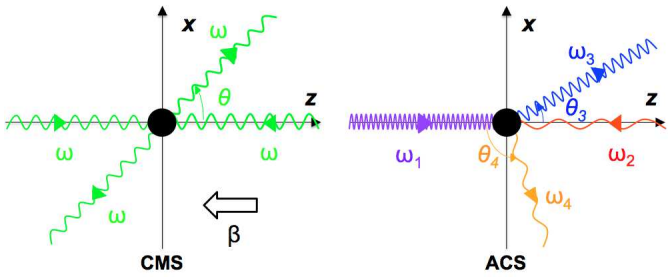

FIG. 1: Asymmetric collision system (ACS) realized in the laboratory frame, interpreted as the result of a Lorentz boost by a relative velocity β of the laboratory frame along the head-on collision (z) axis in the center-of-mass system (CMS). All four photons are confined within a common reaction plane, the x–z plane.

$\omega_1 \equiv u\omega$ and $\omega_2 \equiv u^{-1}\omega$ via the following relationships: $u \equiv \sqrt{(1+\beta)/(1-\beta)} = \gamma + \sqrt{\gamma^2-1}$. With $u^+ \equiv u + u^{-1}$ and $u^- \equiv u - u^{-1}$, energy–momentum conservation results in the following relationships:

$$\begin{aligned} &\text{0-axis:} \quad u^+\omega = \omega_3 + \omega_4, \\ &\text{z-axis:} \quad u^-\omega = \omega_3\cos\theta_3 - \omega_4\cos\theta_4, \\ &\text{x-axis:} \quad \omega_3\sin\theta_3 = \omega_4\sin\theta_4. \end{aligned} \tag{3}$$

We have formulated a QPS with a symmetric incident angle ϑ, which is the half angle between two incident photons when a laser beam with the photon energy $\omega \sim 1$ eV is focused by a lens element. This formulation is also applicable to the CMS. In the coplanar condition whereby the plane determined by $p_1(1)$ and $p_2(1)$ coincides with that determined by $p_3(1)$ and $p_4(1)$ (where the numbers in parentheses specify the linear polarization states), the Lorentz-invariant scattering amplitude of the scalar-field exchange is expressed as

$$\mathcal{M}_S = -(gM^{-1})^2 \frac{\omega^4\left(\cos 2\vartheta - 1\right)^2}{2\omega^2\left(\cos 2\vartheta - 1\right) + m^2}, \tag{4}$$

where the subscript S denotes combinations of linear polarization states of four photons in the initial and final states. The nonzero amplitudes are $\mathcal{M}_{1111} = \mathcal{M}_{2222} = -\mathcal{M}_{1122} = -\mathcal{M}_{2211}$ where the linearly polarized states (1) and (2) are orthogonal to each other. Since all the squared amplitudes are common, we omit the polarization subscript S below. In the following, the denominator of Eq.(4) is denoted by $\mathcal{D}$. We then introduce the imaginary part due to the resonance state by the following replacement:

$$m^2 \to (m - i\Gamma/2)^2 \approx m^2 - im\Gamma, \tag{5}$$

where the decay rate Γ is expressed as

$$\Gamma = (16\pi)^{-1}\left(gM^{-1}\right)^2 m^3 \tag{6}$$

for a given mass m [4]. Substituting this into the denominator in Eq. (4) and expanding around m, we obtain

$$\mathcal{D} \approx -2\left(1 - \cos 2\vartheta\right)(\chi + ia) \;\text{ with }\; \chi = \omega^2 - \omega_r^2, \tag{7}$$

where

$$\omega_r^2 = \frac{m^2/2}{1-\cos 2\vartheta}, \quad a = \frac{m\Gamma/2}{1-\cos 2\vartheta}. \tag{8}$$

Because the scattering amplitude is Lorentz invariant, we have only to consider $\vartheta = \pi/2$ in the above formulation, corresponding to the CMS, in order to apply it to the ACS with the arbitrary parameter u and u^{-1} associated with a Lorentz boost along the head-on collision axis in the CMS. In the CMS, Eq. (8) is thus simplified as

$$\omega_r^2 = \left(\frac{m}{2}\right)^2, \quad a = \frac{m}{4}\Gamma. \tag{9}$$

From Eqs. (6) and (8), a is also expressed as

$$a = \frac{\omega_r^2}{16\pi}\left(\frac{gm}{M}\right)^2, \tag{10}$$

which shows explicitly the proportionality to M^{-2}. The squared amplitude is then expressed as

$$|\mathcal{M}|^2 \approx (4\pi)^2 \frac{a^2}{\chi^2 + a^2}. \tag{11}$$

In the off-resonance case $\chi \gg a$, equivalent to Eq. (4), $|\mathcal{M}|^2$ is largely suppressed because of the factor $a^2 \propto M^{-4}$ for large M. In contrast, in the limit of $\omega \to \omega_r$, $|\mathcal{M}|^2 \to (4\pi)^2$ is expected from Eq. (11). In principle, this is independent of how small $a \propto M^{-2}$ is.

Physically, however, it is difficult to satisfy $\chi = 0$ exactly in the case of an extremely small a because Γ becomes so narrow. A CMS energy uncertainty is caused by momentum (angle) and energy uncertainties originating from the spatial and temporal localizations of the laser fields by the focusing and shortening pulses, respectively. This uncertainty due to the wavy aspect of a photon is unavoidable, even at the level of a pair of photons in principle. For a given uncertainty $\chi_\pm \equiv \pm\eta a$ with $\eta \gg 1$, we still can expect an enhancement from the averaged effect [12] over the uncertainty as follows:

$$\begin{aligned} \overline{|\mathcal{M}|^2} &= \frac{1}{\chi_+ - \chi_-}\int_{\chi_-}^{\chi_+} |\mathcal{M}|^2 d\chi \\ &= \frac{(4\pi)^2}{2\eta a} 2a\tan^{-1}(\eta) = (4\pi)^2\eta^{-1}\tan^{-1}(\eta) \\ &\approx (4\pi)^2\eta^{-1}\frac{\pi}{2} = 8\pi^3\frac{a}{|\chi_\pm|}, \end{aligned} \tag{12}$$

where the approximation is applied to the situation $\eta \gg 1$. By introducing a beam-energy uncertainty $\Delta\omega$ resulting in a bandwidth $\omega_\pm \equiv m/2 \pm \Delta\omega$ in the CMS with respect to the resonance condition $\omega = m/2$, the uncertainty in χ in the CMS is expressed as

$$\chi_\pm = \omega_\pm^2 - (m/2)^2 = \Delta\omega^2 \pm m\Delta\omega \approx \pm m\Delta\omega, \tag{13}$$

where $\Delta\omega^2 \ll m\Delta\omega$ is assumed in the above approximation. Therefore, with Eqs.(6) and (9), the average of the squared scattering amplitude is approximated as

$$\overline{|\mathcal{M}|^2} \approx 8\pi^3\frac{a}{m\Delta\omega} = \frac{\pi^2}{8\Delta\omega}\left(\frac{g}{M}\right)^2 m^3. \tag{14}$$

Compared to the off-resonant case $|\mathcal{M}|^2 \propto a^2$, $\overline{|\mathcal{M}|^2} \propto a$ still has a gain of $a^{-1} \propto M^2$. This is one of the two most promising features of our approach. We note that the uncertainty of the CMS energy is related to the beam-energy uncertainties $\delta\omega_1$ and $\delta\omega_2$ in the ACS (laboratory frame) as follows:

$$\Delta\omega = \sqrt{\omega_1\omega_2}\sqrt{\left(\frac{\delta\omega_1}{\omega_1}\right)^2 + \left(\frac{\delta\omega_2}{\omega_2}\right)^2} \equiv \frac{mR}{\sqrt{2}}, \tag{15}$$

where in the last step we assume that an experiment tunes the beam energies so that they satisfy $2\sqrt{\omega_1\omega_2} = m$ with a common relative energy uncertainty $R \equiv \delta\omega_i/\omega_i$ for $i = 1, 2$. By substituting Eq. (15) into Eq. (14), we eventually express the mass and coupling dependence of the squared scattering amplitude for a given relative-beam-energy uncertainty R as

$$\overline{|\mathcal{M}|^2} \approx \frac{\sqrt{2}\pi^2}{8R}\left(\frac{g}{M}\right)^2 m^2. \tag{16}$$

We then parametrize the differential cross section $d\sigma_{ngb}$ [6] for a pNGB exchange in the ACS (laboratory frame) as

$$d\sigma_{ngb} = \frac{1}{K(\vartheta)2\omega_1 2\omega_2}\overline{|\mathcal{M}|^2} dL_{ips}, \tag{17}$$

where

$$dL_{ips} = (2\pi)^4\delta(p_3+p_4-p_1-p_2)\frac{d^3p_3}{2\omega_3(2\pi)^3}\frac{d^3p_4}{2\omega_4(2\pi)^3} \tag{18}$$

and the relative velocity K is defined as [13]

$$K(\vartheta) \equiv \sqrt{(\vec{v_1}-\vec{v_2})^2 - \frac{(\vec{v_1}\times\vec{v_2})^2}{c^2}} = 2c\sin^2\vartheta = 2 \tag{19}$$

for $\vartheta = \pi/2$ and $\hbar = c = 1$. With $d^3p_3 = |\vec{p_3}|\omega_3 d\omega_3 d\Omega_3$, we can express the differential cross section as a function of the solid angle $d\Omega_3$ of signal photon energy ω_3 as follows:

$$\frac{d\sigma_{ngb}}{d\Omega_3} = \left(\frac{1}{8\pi\omega}\right)^2\left(\frac{\omega_3}{2\omega}\right)^2\overline{|\mathcal{M}|^2} \tag{20}$$

with

$$\omega_3 \equiv \frac{2\omega}{u^+ - u^-\cos\theta_3}, \tag{21}$$

which is a result of energy–momentum conservation.

In what follows, for simplicity, we assume perfect energy resolution of signal photon ω_3 so that we can discuss the momentum range of $\underline{p_3}$ based only on the angular spread of $\vec{p}_3$ from $\underline{\theta_3}$ to $\overline{\theta_3}$ on the reaction plane and $\Delta\phi_3 \equiv \overline{\phi_3} - \underline{\phi_3}$ in the perpendicular direction with respect to the reaction plane in the ACS (see Fig. 2). We

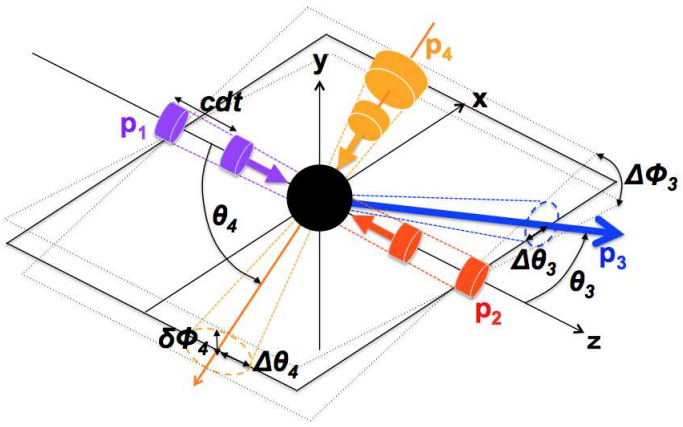

FIG. 2: Collision geometry between three pulsed photon beams. Creation photon pulses p_1 and p_2 collide head-on at the origin of the xyz-coordinates and a coherent laser pulse p_4 to stimulate the scattering is simultaneously focused into the origin. As a result of the stimulated $\gamma\gamma \to \gamma\gamma$ scattering, signal photons p_3 are produced on the same reaction plane. The solid angle of $\vec{p}_3$ enhanced by the inducing beam p_4 is related to the angular spread of $\vec{p}_4$ via energy-momentum conservation. This relationship gives the rotation angle $\Delta\phi_3$ of the reaction plane around the z-axis.

now express the partially integrated cross section $\tilde{\sigma}_{ngb}$ over $d\Omega_3$ in the ACS as follows:

$$\begin{aligned}\tilde{\sigma}_{ngb} &= \frac{\overline{|\mathcal{M}|^2}}{(8\pi\omega)^2}\int_{\underline{\phi_3}}^{\overline{\phi_3}} d\phi_3 \int_{\underline{\theta_3}}^{\overline{\theta_3}}\left(\frac{\omega_3}{2\omega}\right)^2 \sin\theta_3 d\theta_3 \\ &= \frac{\frac{\sqrt{2}\pi^2}{8R}\left(\frac{g}{M}\right)^2 m^2}{(8\pi\omega)^2}\frac{\Delta\phi_3(\cos\underline{\theta_3} - \cos\overline{\theta_3})}{(u^+ - u^-\cos\underline{\theta_3})(u^+ - u^-\cos\overline{\theta_3})} \\ &= \frac{\sqrt{2}}{2(16\omega)^2 R}\left(\frac{gm}{M}\right)^2\mathcal{I} = \frac{\sqrt{2}}{128R}\left(\frac{g}{M}\right)^2\mathcal{I},\end{aligned} \tag{22}$$

where Eqs. (21) and (16) are substituted, and we introduce

$$\mathcal{I} \equiv \frac{\Delta\phi_3(\cos\underline{\theta_3} - \cos\overline{\theta_3})}{(u^+ - u^-\cos\underline{\theta_3})(u^+ - u^-\cos\overline{\theta_3})}. \tag{23}$$

As shown in the last step of Eq. (22), $\tilde{\sigma}_{ngb}$ eventually becomes independent of mass because the beam energies in the ACS are tuned so that $\omega = m/2$ is satisfied in the corresponding CMS.

The second important feature of our approach is to induce a specific two-photon final state by supplying an additional coherent field with a different wavelength ω_4 from any of ω_1, ω_2, or ω_3. Simultaneously, the momentum of the induction field p_4 must coincide with that of one of the two photons in the final state. Therefore, the stimulated range of the signal photon p_3 is determined by the momentum range of the inducing coherent photons p_4 after all. For simplicity, we assume that the momentum spread of p_4 is dominated by the angular spread of $\vec{p}_4$ due to the short focal length of a lens element by neglecting the intrinsic energy spread of ω_4. In this case,

we can express the angular range θ_3 via the third relation in Eq. (3) as

$$\overline{\theta_3} = \sin^{-1}\left(\frac{v}{u^+ - v}\sin(\theta_4 + \Delta\theta_4)\right) \quad (24)$$
$$\underline{\theta_3} = \sin^{-1}\left(\frac{v}{u^+ - v}\sin(\theta_4 - \Delta\theta_4)\right),$$

where $\omega_4 \equiv v\omega$ and $\Delta\theta_4 \sim 1/(2F_4)$ by assuming that the p_4 beam is focused with the f-number F_4 as illustrated in Fig. 2. Figure 2 depicts all the optical beam axes as being on a common reaction plane, and p_4 is provided as a cone-like focused beam based on Gaussian optics. Therefore, a slight deviation of $\vec{p}_3$ from the coplanar condition is determined by the angular spread of $\vec{p}_4$. This azimuthal angular spread, $\delta\phi_4$, of $\vec{p}_4$ from the reaction plane gives the rotation angles of the reaction planes around the z axis. Hence, we can express $\Delta\phi_3$ as

$$\Delta\phi_3 = 2\sin^{-1}\left(\frac{\sin\delta\phi_4}{\sqrt{\sin^2\theta_4\cos^2\delta\phi_4 + \sin^2\delta\phi_4}}\right), \quad (25)$$

where $\delta\phi_4 = \Delta\theta_4$ holds because of the axial symmetry around the optical axis of the p_4 beam. By substituting these parameters into Eq. (23), we can evaluate an inducible partially integrated cross section from Eq. (22).

With the parametrization for signal yield, $\mathcal{Y}$, developed in Appendix A of Ref. [6], we express the expected number of signals with ω_3 per pulse crossing for the spontaneous scattering process as

$$\mathcal{Y}_s = \int dt \int dx^i \rho_1(t,x^i)\rho_2(t,x^i) K\left[1/L^2\right]\tilde{\sigma}_{ngb}\left[L^2\right], \quad (26)$$

where i runs from 1 to 3, and the first factor corresponds to time integrated beam luminosity with the dimension of $1/L^2$ with length unit L. We then express the induction effect by convoluting the probability distribution function of an induction field P_4 as follows:

$$\mathcal{Y}_i = \int dt \int dx^i \rho_1(t,x^i)\rho_2(t,x^i) K\tilde{\sigma}_{ngb} P_4(t,x^i) \quad (27)$$
$$\equiv K\tilde{\sigma}_{ngb} N_1 N_2 N_4 G,$$

where ρ_k indicates a normalized density distribution over an infinite space-time range for creation beams $k = 1, 2$ and the induction beam $k = 4$ by assuming pulsed Gaussian beams with the number of photons contained in individual pulses, N_1, N_2, and N_4, as defined explicitly in the following. The factor G is the integrated geometrical overlap factor. At a space point x^i for a given common time t in the ACS, the squared field strength of a Gaussian laser pulse can be parametrized as [14]

$$I(x, y, z = ct) = E_0^2 \frac{w_0^2}{w^2(ct)} e^{-2\frac{x^2+y^2}{w^2(ct)}} e^{-2\left(\frac{z-ct}{c\tau}\right)^2}, \quad (28)$$

where E_0 is the electric field and E_0^2 is proportional to the number of photons N in a pulse, τ is the pulse duration time, and the beam radius $w(ct) = w_0\sqrt{1 + (ct/Z_R)^2}$ is given for wavelength λ, beam waist $w_0 = 2F\lambda/\pi$, and Rayleigh length $Z_R = \pi w_0^2/\lambda$. The volume for the normalization is thus obtained as

$$V = \int_{-\infty}^{\infty} \frac{I(x^i)}{E_0^2} dx^i = (\pi/2)^{3/2} w_0^2 c\tau. \quad (29)$$

Based on the three-beam arrangement in the identical reaction plane in Fig .2, the normalized densities $\rho_k = I_k/V_k$ are defined as follows:

$$\rho_1(x^i) = N_1 \frac{(2/\pi)^{3/2}}{w_1^2(ct)c\tau_1} e^{-2\frac{x^2+y^2}{w_1^2(ct)}} e^{-2\left(\frac{z-ct}{c\tau_1}\right)^2}, \quad (30)$$
$$\rho_2(x^i) = N_2 \frac{(2/\pi)^{3/2}}{w_2^2(ct)c\tau_2} e^{-2\frac{x^2+y^2}{w_2^2(ct)}} e^{-2\left(\frac{z+ct}{c\tau_2}\right)^2},$$
$$P_4(x^i) = V_4\rho_4(x^i) = N_4 \frac{w_{04}^2}{w_4^2(ct)} e^{-2\frac{X^2+y^2}{w_4^2(ct)}} e^{-2\left(\frac{Z-ct}{c\tau_4}\right)^2},$$

where $X \equiv \sin(\pi+\theta_4)x + \cos(\pi+\theta_4)z$ and $Z \equiv \cos(\pi+\theta_4)x - \sin(\pi+\theta_4)z$ are introduced for the rotated incidence of the coherent induction field with respect to the head-on collision axis of the ACS.

The geometrical overlap factor integrated over the longest pulse duration τ_L among the three pulses whose central positions are all at the origin at $t = 0$ is then expressed as

$$G = (2/\pi)^{3/2}(w_{04}/(c\tau))^2 \int_{-\tau_L}^{\tau_L} dt (w_1 w_2 w_4)^{-2} \times \quad (31)$$
$$\{A(1/w_1^2 + 1/w_2^2 + 1/w_4^2)B\}^{-1/2} e^{-2Dt^2},$$

where for simplicity we assume that experiments introduce $\tau = \tau_1 = \tau_2$ with

$$A \equiv 1/w_1^2 + 1/w_2^2 + (\cos\theta_4/w_4)^2 + (\sin\theta_4/(c\tau_4))^2,$$
$$B \equiv (\sin\theta_4/w_4)^2 + (\cos\theta_4/(c\tau_4))^2 + 2/(c\tau)^2 -$$
$$[\sin\theta_4\cos\theta_4\{1/w_4^2 - 1/(c\tau_4)^2\}]^2/A,$$
$$D \equiv 2/\tau^2 + 1/\tau_4^2 - \left[\sin^2\theta_4/A + \right.$$
$$\left.\cos^2\theta_4\{1 + (1/w_4^2 - 1/(c\tau_4)^2)\sin^2\theta_4\}^2/B \ \right]/(c\tau_4^2)^2.$$

Because the total number Y of detected signal photons is described as $Y = fT\epsilon\mathcal{Y}_i$ with collision repetition rate f [Hz], data accumulation time T [s], and detection efficiency ϵ, a reachable coupling strength is finally expressed as

$$\frac{g}{M} = 2^{1/4} 8 \sqrt{\frac{RY}{\mathcal{I} f T \epsilon K G N_1 N_2 N_4}} \quad (32)$$

from Eqs. (22) and (27). We note that g/M has m^{-1} dependence because $G \propto \omega^2 \propto m^2$.

III. SENSITIVITY AND QED BACKGROUND

The three dashed lines in Fig. 3 show g/M [1/GeV] as a function of m [eV] for $N_k = 10^{10}, 10^{15}$, and 10^{20} for

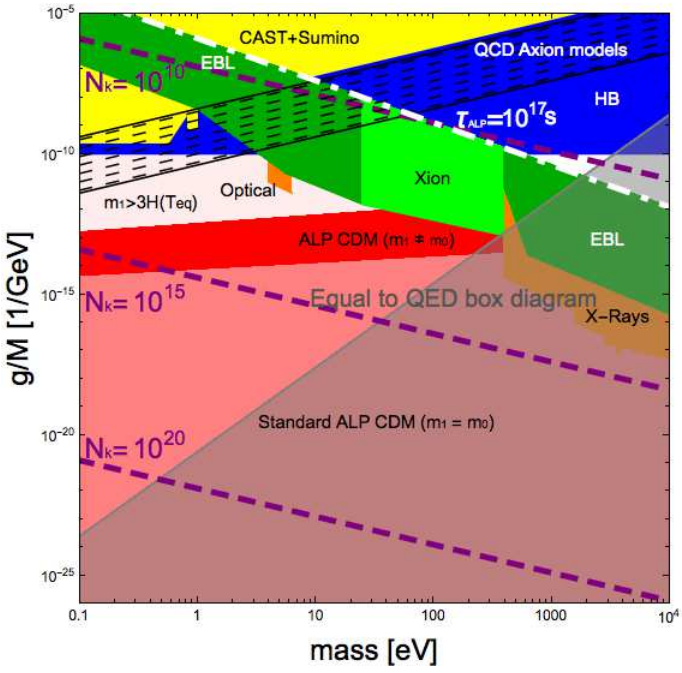

FIG. 3: Sensitivity to the mass–coupling domains. Experimentally excluded and theoretically predicted domains are all imported from Ref. [16], where all details are explained. A natural constraint that the lifetime of dark matter is equal to the age of the universe at the shortest is expressed as the dash-dotted line. The three dashed lines show accessible coupling limits with $N_k = 10^{10}, 10^{15}, 10^{20}$ common for $k = 1, 2, 4$, respectively based on Eq. (32) for the common parameter set in Table I. This figure shows the domain in which the QED process dominates the cross section of a pNGB exchange observed by the same method. The boundary line of the gray translucent area shows m–g/M, at which $\tilde{\sigma}_{ngb} = \tilde{\sigma}_{qed}$ is satisfied.

$k = 1, 2, 4$, respectively based on Eq. (32) in the range 0.1 eV to 10 keV. The experimentally excluded and theoretically expected domains of the mass–coupling relationship are imported from Ref. [16], where all details are explained. For this figure, the set of parameters summarized in Table I is assumed, where the parameters in the upper rows can be commonly used for any $\omega = m/2$. We note here that a long f-number F is assumed deliberately, thereby guaranteeing that the CMS energy does not fluctuate because of the uncertainty in the incident angles but rather because of the energy spread of the creation beams. This allows the use of nearly parallel incoherent creation pulses, for instance, those generated by laser-electron Compton scattering, as we discussed in all-optical-based γ–γ scattering [18]. As an example of ω, we show concrete energies and scattering angles in the second set of rows if we aim at $m = 7$ keV in order to test the possibility of pNGB exchange to explain the excess [8].

Above the keV range, we must take photon–photon scattering based on quantum electrodynamics (QED) into account as a background source from the standard model. Probing QED-based photon–photon scattering via four-wave mixing has been proposed in Ref. [17]. These calculations are based on the Euler–Heisenberg effective Lagrangian and the signal yield is evaluated within a classical wave picture. The formulation we provide here is based on the particle picture of colliding photons and thus allows us to simply plug the partially integrated cross section, $\tilde{\sigma}_{qed}$, for the QED box diagram into Eq. (27), which has been applied to $\tilde{\sigma}_{ngb}$ on the same footing. The differential cross section of the elastic QED scattering process [15] with respect to scattering angles in the ACS is expressed as

$$d\sigma_{qed} = \frac{(\alpha r_0)^2}{4\pi^2}\frac{139}{90^2}\omega^6\left(3+\frac{\gamma^2(\cos\theta_3-\beta)^2}{\gamma^2(\cos\theta_3-\beta)^2+\sin^2\theta_3}\right)^2 \times \left(1+\frac{160}{139}\frac{\omega^2\sin^2\theta_3}{4\gamma^2(\cos\theta_3-\beta)^2+3\sin^2\theta_3}\right)\times \sqrt{\frac{\sin^2\theta_3}{\gamma^2(\cos\theta_3-\beta)^2+\sin^2\theta_3}}\frac{\gamma(1-\beta\cos\theta_3)}{\gamma^2(\cos\theta_3-\beta)^2+\sin^2\theta_3}d\theta_3 d\phi_3 \quad (33)$$

with $\alpha = 1/137$ and $r_0 = 2.8\times10^{-13}$ cm. This corresponds to the unpolarized case that is comparable to the s-channel scalar-pNGB exchange with $S = 1111$ discussed here, because the $S = 1111$ cross section eventually coincides with that of the unpolarized photon–photon scattering. Since the solid angle and the effect of the induction laser field are common to both the pNGB exchange and the QED process, we have only to plug the partially integrated QED cross section into Eq. (27) in order to get the QED-based scattering yield. The boundary line of the gray translucent area in Fig.3 shows m–g/M, at which $\tilde{\sigma}_{ngb} = \tilde{\sigma}_{qed}$ is satisfied. This equi-cross-section line intersects with the constraint from a natural requirement that the life time of a pNGB is equal to the age of the universe [3] at around $(m, g/M) = (2\text{ keV}, 10^{-11}\text{ GeV}^{-1})$. Although the QED cross section exceeds the pNGB cross section consistent with a natural dark matter candidate (dash-dotted line) at m=7 keV, the search window of $m < 2$ keV is still wide-open with relatively low QED background levels.

IV. LIGHT SOURCES

There are already several short-pulsed coherent/incoherent light sources that cover the range 0.1 eV to 10 keV. In the 1–10 keV range, free-electron lasers are already available. For instance, an X-ray free-electron laser (XFEL), SACLA [19], can provide $N_k \sim 10^{11}$ at $f = 60$ Hz in that energy range with an undulator length of 90 m. Although introducing three long XFEL lines would likely be difficult from a practical point of view, incoherent photon–photon collisions for only the creation part combined with an XFEL for the stimulation part would be the least time-consuming approach. This is because incoherent light sources can be attainable using relatively compact

Lorentz factor to boost CMS energies	$\gamma = 1.5$
Scattering angle in CMS	$\theta = \pi/4$
Incident angle of induction beam	$\theta_4 = 1.65$ rad
Scattering angle of signal photons	$\theta_3 = 0.31$ rad
Common f-number of creation beams	$F = 100$
Induction beam f-number	$F_4 = 10$
Common duration time for creation beams	$\tau = Z_{R2}/c$
Integration time from longest Rayleigh length	$\tau_L = Z_{R2}/c$
Common energy uncertainty of creation beams	$R = 5\%$
Collision repetition rate	$f = 1$ Hz
Data accumulation time	$T = 10^6$ s
Total number of signal photons	Y = 100
Detector efficiency to signal photons	$\epsilon = 100\%$
Creation beam energy in CMS	$\omega = 3.50$ keV
Higher creation beam energy in ACS	$\omega_1 = 9.16$ keV
Lower creation beam energy in ACS	$\omega_2 = 1.34$ keV
Induction beam energy in ACS	$\omega_4 = 2.48$ keV
Signal photon energy in ACS	$\omega_3 = 8.02$ keV

TABLE I: Three-beam parameters in CMS and ACS (laboratory frame). The second set of rows gives example values when tuned at $m = 2\omega = 7$ keV.

all-optical laser systems [18]. In addition, such a long-scale undulator might be drastically shortened by future developments in compact coherent X-ray sources, such as a graphene-based undulator [21]. In the 10 eV–1 keV range, the generation of higher harmonics by shooting high-intensity laser pulses into material targets could be useful [20]. In the 0.1–10 eV range, variable-wavelength lasers based on optical parametric amplification are available as commercial products. State-of-the-art laser facilities such as the Extreme Light Infrastructure [22] can reach numbers of optical coherent photons per pulse beyond $N_k \sim 10^{20}$ with $\tau_L \sim 10$ fs. These facilities can generate multi-wavelength laser fields up to the keV range with high intensity by combining several of the methods mentioned above.

V. CONCLUSION

We formulated a stimulated photon–photon scattering process via an s-channel pNGB exchange in an asymmetric head-on collision system that would be applicable to the mass range of 0.1 eV to 10 keV. Above $m = 2$ keV, we found that the QED photon–photon scattering cross section dominates that of a pNGB exchange whose lifetime is consistent with the age of the universe. Especially in the 0.1-100 eV range, the domain with $g/M < 10^{-12}$ GeV^{-1} has not been tested against any observations to date. Therefore, the proposed method could provide a wide search window onto an unexplored valley in the sensitivity curve with relatively suppressed QED background levels. The sensitivity could eventually reach the domain beyond the GUT scale $M \sim 10^{16}$ GeV, hence, our proposal could provide opportunities to test string-theory-based models [23].

It would be valuable for future experiments to tune the beam energy and intensity so that the expected sensitivity could reach the equi-cross-section line. Confirmation of the QED process is firstly important to guarantee that the experiment is indeed performing properly. Once the QED scattering has been confirmed, it would be interesting to test whether interference exists between the pNGB exchange and the QED process, for example, by looking at the angular distribution of the signal photons by changing the incident angle of the induction laser beam and also the dependence on the combination of linear polarization states. By repeating this test over four orders of magnitude in the CMS energies, if we were to see a statistically significant deviation from the QED prediction in a particular mass range, we could reduce the laser intensity at which the QED effect becomes insignificant. If we still see the scattering phenomenon, we would be able to claim that something dark is exchanged in the photon–photon scattering process.

Acknowledgments

We thank Y. Fujii for helpful discussions. K. Homma acknowledges the support of the Collaborative Research Program of the Institute for Chemical Research, Kyoto University (Grants Nos. 2016–68) and the Grants-in-Aid for Scientific Research Nos. 15K13487 and 16H01100 from MEXT of Japan.

[1] R. D. Peccei and H. R. Quinn, Phys. Rev. Lett **38**, 1440 (1977); S. Weinberg, Phys. Rev. Lett **40**, 223 (1978); F. Wilczek, Phys. Rev. Lett **40**, 271 (1978).
[2] Y. Fujii and K. Maeda, *The Scalar-Tensor Theory of Gravitation* Cambridge Univ. Press (2003).
[3] A. Arvanitaki, S. Dimopoulos, S. Dubovsky, N. Kaloper, and J. March-Russell, Phys. Rev. D **81**, 123530 (2010); B. S. Acharya, K. Bobkov, and P. Kumar, J. High Energy Phys. **11**, 105 (2010); M. Cicoli, M. Goodsell, and A. Ringwald, J. High Energy Phys. **10**, 146 (2012).
[4] Y. Fujii and K. Homma, Prog. Theor. Phys **126**, 531 (2011); Prog. Theor. Exp. Phys. 089203 (2014) [erratum].
[5] S. A. J. Druet and J.-P. E. Taran, Prog. Quant. Electr. **7**, 1 (1981).

[6] K. Homma, T. Hasebe, and K.Kume, Prog. Theor. Exp. Phys. 083C01 (2014).

[7] T. Hasebe, K. Homma, Y. Nakamiya, K. Matsuura, K. Otani, M. Hashida, S. Inoue, S. Sakabe, Prog. Theor. Exp. Phys. 073C01 (2015).

[8] E. Bulbul et al., Astrophys. J. **789**, 13 (2014).

[9] A. Boyarsky, O. Ruchayskiy, D. Iakubovskyi and J. Franse, Phys. Rev. Lett. **113**, 251301 (2014).

[10] E. Bulbul, M. Markevitch, A. Foster, E. Miller, M. Bautz, M. Loewenstein, S. W. Randall and R. K. Smith, Astrophys. J. **831**, 55 (2016) ; F. A. Aharonian *et al.* [Hitomi Collaboration], arXiv:1607.07420 [astro-ph.HE] ; J. P. Conlon, F. Day, N. Jennings, S. Krippendorf and M. Rummel, arXiv:1608.01684 [astro-ph.HE].

[11] J. Jaeckel, J. Redondo and A. Ringwald, Phys.Rev. D **89**, 103511 (2014).

[12] On a similar treatment for a narrow resonance case, see Eq. (49.1) in C. Patrignani et al. (Particle Data Group), Chin. Phys. C **40**, 100001 (2016).

[13] M. A. Furman, LBNL-53553, CBP Note-543.

[14] Amnon Yariv, *Optical Electronics in Modern Communications* (Oxford University Press, Inc. 1997).

[15] B. De Tollis, Nuovo Cimento **32**, 757 (1964); B. De Tollis, Nouvo Cimento **35**, 1182 (1965).

[16] P. Arias, D. Cadamuro, M. Goodsell, J. Jaeckel, J. Redondo, and A. Ringwald, JCAP **06**, 013 (2012).

[17] F. Moulin and D. Bernard, Opt. Commun. 164, 137 (1999); E. Lundström et al., Phys. Rev. Lett. **96**, 083602 (2006); J. Lundin et al., Phys. Rev. A **74**, 043821 (2006); D. Bernard et al., Eur. Phys. J. D **10**, 141 (2000).

[18] K. Homma, K. Matsuura, and K. Nakajima, Prog. Theor. Exp. Phys. 083C01 (2014).

[19] T. Ishikawa et al., Nature Photonics **6**, 540 (2012).

[20] T. Popmintchev et al., Science **336**, 1287 (2012).

[21] L. J. Wong, I. Kaminer, O. Ilic, J. D. Joannopoulos, and M. Soljačić, Nature Photonics **10**, 46 (2016).

[22] http://www.eli-laser.eu/

[23] P. Svrcek and E. Witten, J. High Energy Phys. **0606**, 051 (2006).